Rock and Soil Mechanics

Volume 44 | Issue 5 Article 8

8-21-2023

Infiltration characteristics and deformation mechanism of rainfall-induced landslides in Three Gorges Reservoir Area based on 1D and 2D model tests

Li WANG
Key Laboratory of Geological Hazards on Three Gorges Reservoir Area, Ministry of Education, China Three Gorges University, Yichang, Hubei 443002, China, College of Civil Engineering & Architecture, China Three Gorges University, Yichang, Hubei 443002, China, Badong National Observation and Research Station of Geohazards, China University of Geosciences, Wuhan, Hubei 430074, China

Fang-yun NAN
Key Laboratory of Geological Hazards on Three Gorges Reservoir Area, Ministry of Education, China Three Gorges University, Yichang, Hubei 443002, China, College of Civil Engineering & Architecture, China Three Gorges University, Yichang, Hubei 443002, China

Shi-mei WANGi
Key Laboratory of Geological Hazards on Three Gorges Reservoir Area, Ministry of Education, China Three Gorges University, Yichang, Hubei 443002, China, College of Civil Engineering & Architecture, China Three Gorges University, Yichang, Hubei 443002, China

Yong CHEN
Key Laboratory of Geological Hazards on Three Gorges Reservoir Area, Ministry of Education, China Three Gorges University, Yichang, Hubei 443002, China, College of Civil Engineering & Architecture, China Three Gorges University, Yichang, Hubei 443002, China

Recommended Citation

See next page for additional authors
WANG, Li; NAN, Fang-yun; WANGi, Shi-mei; CHEN, Yong; LI, Xiao-wei; FAN, Zhi-hong; and CHEN, Yu-shan (2023) "Infiltration characteristics and deformation mechanism of rainfall-induced landslides in Three Gorges Reservoir Area based on 1D and 2D model tests," *Rock and Soil Mechanics*: Vol. 44: Iss. 5, Article 8.
DOI: 10.16285/j.rsm.2022.00248
Available at: https://rocksoilmech.researchcommons.org/journal/vol44/iss5/8

Infiltration characteristics and deformation mechanism of rainfall-induced landslides in Three Gorges Reservoir Area based on 1D and 2D model tests

Authors

Li WANG, Fang-yun NAN, Shi-mei WANGi, Yong CHEN, Xiao-wei LI, Zhi-hong FAN, and Yu-shan CHEN

Rock and Soil Mechanics 2023 44(5): 1363−1374 ISSN 1000−7598
https: //doi.org/10.16285/j.rsm.2022.00248 http://rocksoilmech.researchcommons.org/journal

Infiltration characteristics and deformation mechanism of rainfall-induced landslides in Three Gorges Reservoir Area based on 1D and 2D model tests

WANG Li[1, 2, 3], NAN Fang-yun[1, 2], WANG Shi-mei[1, 2], CHEN Yong[1, 2], LI Xiao-wei[4], FAN Zhi-hong[1, 2], CHEN Yu-shan[1, 2]

1. Key Laboratory of Geological Hazards on Three Gorges Reservoir Area, Ministry of Education, China Three Gorges University, Yichang, Hubei 443002, China
2. College of Civil Engineering & Architecture, China Three Gorges University, Yichang, Hubei 443002, China
3. Badong National Observation and Research Station of Geohazards, China University of Geosciences, Wuhan, Hubei 430074, China
4. Central-South Institute of Metallurgical Geology, Yichang, Hubei 443002, China

Abstract: Shallow deformation of ancient landslides induced by heavy rainfall is the most serious geological disaster in China's Three Gorges Reservoir Area (TGRA). It is important to explore the infiltration characteristics and its shallow deformation mechanism caused by heavy rainfall. In this study, the rainfall-induced landslide of the TGRA was selected as the research object, and the distributions of the soil permeability coefficients for rainfall-type landslide were summarized. Considering the effects of heavy rainfall, one-dimensional (1D) soil column infiltration test and two-dimensional (2D) landslide model test were conducted to study the infiltration characteristics of landslide soil and the corresponding shallow deformation mechanisms under different rainfall intensities. The results of the rainfall infiltration tests show that the speed of rainfall infiltration into soil depends on the magnitudes of rainfall intensity and soil permeability coefficient, i.e. when the rainfall intensity is less than or equal to the soil permeability coefficient, the infiltration capacity increases with rainfall intensity; when the rainfall intensity is greater than the soil permeability coefficient, the infiltration capacity decreases. The model test results show that the infiltration of heavy rainfall makes the surface soil transiently saturated and then the gas in the unsaturated zone below the surface is temporarily closed, which leads to the compression of gas by the surface pore water pressure. This means that the pore gas pressure increases with the infiltration of heavy rainfall. Overall, for the rainfall-induced landslides in TGRA, short-term torrential rain can create transient saturation zones and generate closing gas which is the main reason affecting the infiltration capacity of heavy rainfall. The water pressure transmitted by the closing gas causes the pore water pressure of the shallow soil to increase sharply, which is also the main reason for the shallow deformation and damage of many landslides.

Keywords: Three Gorges Reservoir Area; model test; rainfall-induced landslides; infiltration characteristics; deformation mechanism

1 Introduction

The Three Gorges Reservoir Area (TGRA) is located in the upper reaches of the Yangtze River in China, from Chongqing in the west to Yichang in the east (Fig.1(a)), with a length of 660 km[1]. More than 5000 landslides have occurred in the TGRA[2]. Therefore, many researchers have noted that the long-term rise and fall of the reservoir water level may cause a large number of landslide cases[1, 3–4]. However, to date, there are no relevant reports of landslide events caused by water storage in the TGRA. Rainfall remains the most important factor that induces the landslide events in the TGRA[2], especially the short-term extreme rainfall, which has triggered a wide range of landslide deformation events throughout history[5–6]. The vast majority of landslide deformation events are the shallow type induced by heavy rainfall, causing huge economic losses and casualties. Therefore, understanding the infiltration characteristics and deformation mechanism of landslides under heavy rainfall is important for disaster prevention and mitigation of landslides in the TGRA.

Existing studies have a common understanding of the mechanism of rainfall-induced landslides, i.e. rainfall infiltration leads to an increase in soil water content, which reduces the soil shear strength[7], increases the pore water pressure, softens the sliding surface of the landslide, and induces the landslide[8]. However, this basic understanding requires further investigation. For example, for the landslides with thicker soil layers, rainwater infiltration does not significantly affect the sliding surface, and under heavy rainfall, many landslides actually experience shallow sliding[9]. For the same type of sliding soil, whether the infiltration characteristics under different rainfall

Received: 26 September 2022 Accepted: 30 December 2022
This work was supported by the National Natural Science Foundation of China (No. U21A2031), Key R & D Program of Hubei Province (No. 2022BAA047), China Postdoctoral Science Foundation (No.2021M701969), Open Fund of Key Laboratory of Geological Hazards on Three Gorges Reservoir Area (2022KDZ19) and the Open Fund of Badong National Observation and Research Station of Geohazards (No. BNORSG-202207).
First author: WANG Li, male, born in 1988, PhD, research interests: geological disaster mechanisms and geotechnical basic theories. E-mail: wangli_ctgu@126.com
Corresponding author: WANG Shi-mei, female, born in 1965, PhD, Professor, research interests: geological disaster prediction and evaluation. E-mail: shimeiwang1965@126.com

intensities are consistent or there are differences in the landslide deformation mechanism still needs to be investigated.

There are three approaches to investigate these scientific questions. The first approach uses the numerical methods[10], which are very efficient for quickly discussing the influence of different factors on the landslide stability, such as the geological conditions of the landslide[11] and the influences of external conditions including rainfall intensity, duration, pattern, and net rainwater infiltration[12−14]. However, numerical methods are excessively dependent on mature theoretical models and the reliability of the physico-mechanical parameters of rock and soil, and thus it is difficult to gain a new understanding. The second approach is the indoor model test, which is a very reliable method[15−16]. Researchers often pursue geometric[17], physical, material[18], and gravitational similarities[19−20] to achieve the same results as the actual landslide prototype through a model test. When we consider all the factors close to the actual landslide prototype, the realization of the model test becomes extremely difficult. The third approach is to conduct on-site monitoring of landslides[21−22]. With the continuous development of monitoring technology and equipment, this becomes the most commonly used method. For the studies of shallow landslide failure, matric suction[23], soil water content[2, 9], and pore water pressure[24−25] are the commonly used monitoring indicators. Among these, field model test is a special method. In the field model test, suitable natural slopes are selected, monitoring devices and rainfall devices are installed, and artificial rainfall is used until the slope deforms to obtain effective monitoring data[26]. The most reliable data for the response to landslide deformation can be obtained using on-site landslide monitoring techniques. However, this method can only reveal the deformation mechanism of a specific landslide under certain rainfall conditions. Owing to the complexity of landslide composition and the diversity of rainfall conditions, the results obtained are difficult to popularize and apply to other cases.

Considering the aforementioned research, this study investigates the rainfall-induced landslides in the TGRA, counts the distribution of the infiltration characteristics of rainfall-induced landslides, and selects the sliding soil mass with the most concentrated distribution of permeability coefficients as the test material. Considering the effects of heavy rainfall, one-dimensional (1D) soil column infiltration and two-dimensional (2D) landslide model tests are conducted to explore the infiltration characteristics of sliding soil mass under different ratios of rainfall intensity to soil permeability coefficient (q/k) and the corresponding shallow landslide deformation mechanisms. The results obtained in this study provide a theoretical reference for a more comprehensive understanding of the instability mechanism of rainfall-induced landslides in the TGRA and offer a scientific basis for disaster prevention and mitigation of landslides in the TGRA.

2 Rainfall-induced landslides in the TGRA

2.1 Landslides in the TGRA

According to the incomplete statistics, more than 500 large landslides with a volume larger than 100×10^4 m^3 have occurred in the TGRA (Fig. 1(b)), accounting for more than 10% of the total number of landslides, and small landslides account for the largest proportion (more than 60%). In terms of the distribution of the landslide events, the counties (districts) with more than 200 landslides in the TGRA are listed in the following order: Zigui County > Badong County > Wanzhou District > Wulong County > Yunyang County > Fengdu County. In Zigui County, the number of landslides registered is 514; the giant and large landslides also rank in the forefront among the 19 counties (districts) in the reservoir area, including 18 giant landslides and 107 large landslides, accounting for 24.31% of the total number of landslides in this county. The giant and large landslides have also developed in Yiling, Badong, Wushan, Fengjie, Yunyang, Zhongxian, and Fengdu counties. According to the material composition, soil landslides (including accumulated layers and clayey loess landslides) in the TGRA account for 51.15% of the total number of landslides, rock–soil mixed landslides account for 32.75%, and rock landslides account for 16.10%.

The TGRA has a humid climate with abundant rainfall and continuous torrential rains. Landslides induced by atmospheric rainfall account for 71.58% of the total landslides, earthquake-induced landslides account for only 0.31%, landslides caused by human engineering activities account for 2.61%, and the remaining 25.5% are landslides of unknown origin. Considering the abundant data on landslides with a volume greater than 100×10^4 m^3 and their great damage, this study takes this type of landslide as the research object to study the deformation mechanism of rainfall-induced landslides in the TGRA.

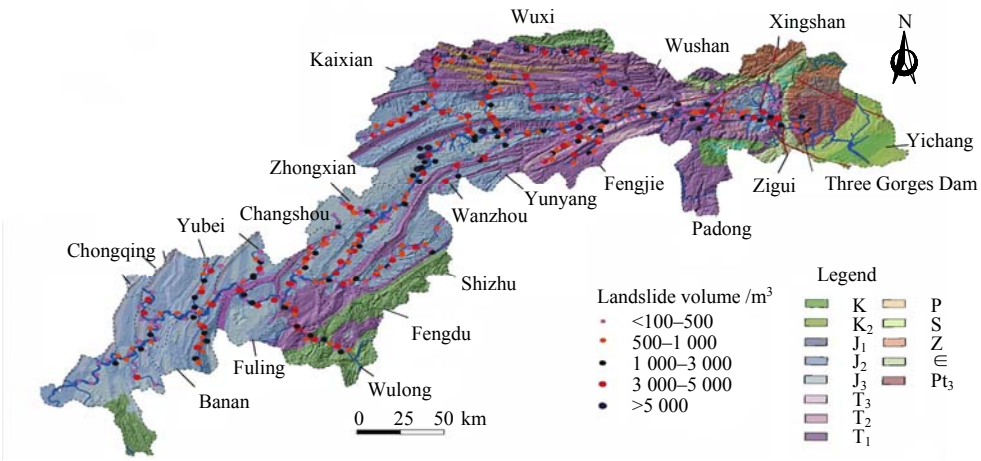

Fig. 1 Distributions of landslides with a volume greater than 1 million m³ in the TGRA (base map fromTang et al.[1])

2.2 Rainfall-induced landslides in the TGRA

The TGRA has a humid climate with abundant rainfall, which is significantly affected by seasons, and it belongs to the subtropical monsoon climate region. The distribution of the total annual rainfall in the TGRA is shown in Fig.2(a). The average annual rainfall in the area is unevenly distributed, ranging from 996.7 mm to 1204.3 mm in the basin area, 992.5 mm to 1241.8 mm in the valley area, and 1 600-2 000 mm in the mountains on both sides of the valley; the rainfall is relatively concentrated. Rainfall in the reservoir area is mostly heavy rains and rainstorms, and approximately 70% of the annual rainfall occurs from May to September, as shown in Fig. 2(b).

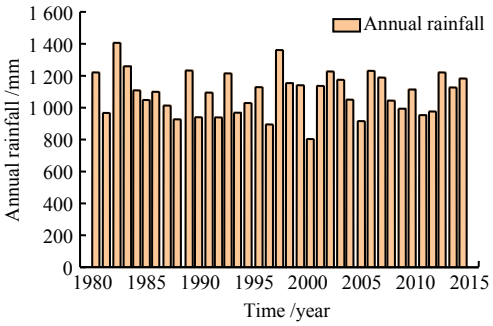

(a) Annual rainfall

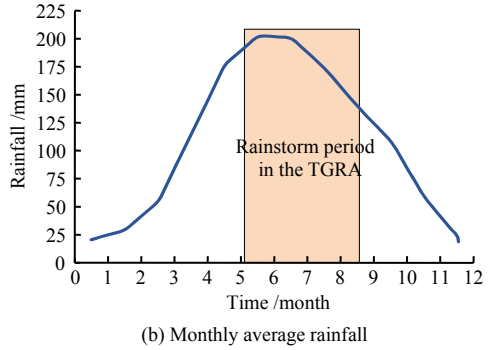

(b) Monthly average rainfall

Fig. 2 Precipitation in the TGRA (1980–2015, data from Wuhan Rainstorm Research Institute, China Meteorological Administration)

Many studies have shown that the frequent occurrence of landslide disasters in the TGRA is strongly related with the abundant rainfall in the region[27]. Short-term heavy rainfall events are rare, such as the extremely heavy rainfall event that occurred on August 31, 2014. This rainstorm lasted from 08:00 on August 31, 2014 to 14:00 on September 2, 2014, a total of 54 h, and the maximum daily rainfall was 385 mm, causing a total of 1039 landslide disasters in the TGRA. Long-term light rainfall also has serious influence. For example, in the "Autumn Rain of West China" in 2017, the cumulative precipitation amount was the largest since 1984, resulting in hundreds of disasters occurring in Zigui and Badong counties[2].

The above data show that the heavy rainfall has a significant impact on the stability of landslides in the TGRA. The landslide-prone areas in the TGRA, such as Zigui, Badong, Yunyang, and Wanzhou counties, are located in the rainfall center[1]. Considering the relationship between rainfall and landslides in the above-mentioned areas, the management department concluded that continuous rainfall more than or equal to 3 d, with a rainfall of 270–300 mm, can induce small bedrock landslides; continuous rainfall more than or equal to 2 d, with a rainfall of 280–300 mm, can reactivate the old small and medium-sized landslide remnants; and continuous rainfall more than or equal to 6 d, with a rainfall of 480–510 mm, can trigger large and medium-sized bedrock landslides. However, these conclusions, based on the empirical data, are difficult to apply to actual landslide early-warnings, and the relationship between rainfall and landslide deformation in the TGRA needs further investigation.

2.3 Permeability characteristics of rainfall-induced landslides

In this study, we collect 240 rainfall-induced

landslides with the volume more than 1 million m³. The soil types of the landslides are silty clay, silty clay mixed with gravel, and gravel soil. Based on these soils, field pit tests (refer to standard test methods for field measurement of hydraulic conductivity ASTM D6391−11[28]) and indoor penetration tests are conducted, and the penetration test results of 240 landslide soils are determined. The distribution ranges are shown in Fig. 3.

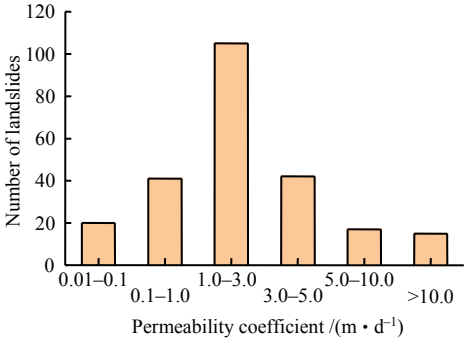

Fig. 3 Distribution ranges of permeability coefficients for landslide soil in the TGRA

One can see from the statistical results in Fig. 3 that the permeability coefficient of rainfall-induced landslides in the TGRA ranges from 0.1 m/d to 5.0 m/d, showing a good permeability. Nearly 50% of the landslide soil permeability coefficients are distributed between 1.0 m/d and 3.0 m/d, which is the main range of the permeability coefficients considered in the model test in this study.

3 Model test design

3.1 Test device

Based on the infiltration characteristics of rainfall-induced landslides in the TGRA, this study conducts a 1D soil column infiltration test combined with a 2D landslide model test to investigate the infiltration characteristics and deformation mechanism of rainfall-induced landslides.

Figure 4(a) shows the photo of the 1D soil column infiltration test device, and Fig.4(d) shows the corresponding schematic diagram. A glass cylinder is used to prepare the test soil column. The soil column infiltration test device consists of three plexiglass columns, one set of rainfall devices, one set of camera devices, and several rubber hoses. The inner diameter of the cylinder is 500 mm, its height is 500 mm, and there is a faucet with an outer diameter of 25 mm at the bottom. Fig. 4(b) shows the rainfall control system, which consists of a rainfall controller, conduit, and nozzle. Figure 4(c) shows the 2D model test device, and Fig. 4(e) shows the corresponding schematic diagram, which is mainly composed of a model frame, rainfall frame, and rainfall device. The model frame is 4 m long, 2 m wide, and 1 m high. The effective rainfall height of the rainfall device is 2–4 m, and the continuous variation range of rainfall intensity is 10–200 mm/h.

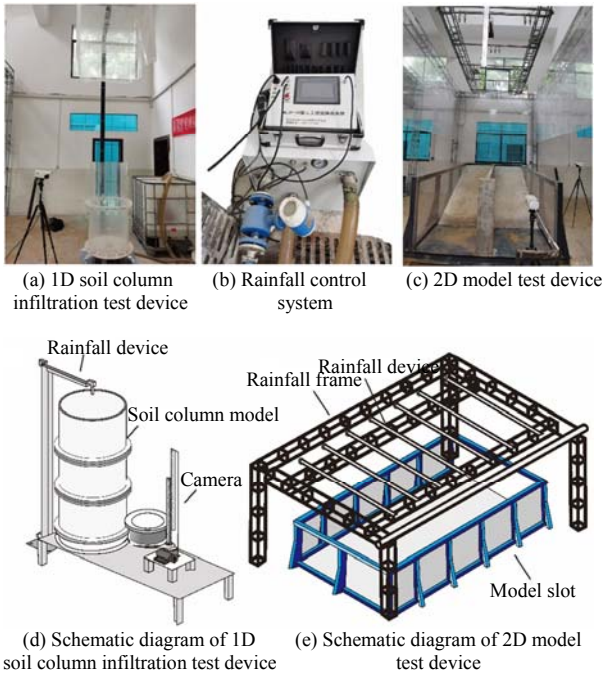

(a) 1D soil column infiltration test device (b) Rainfall control system (c) 2D model test device

(d) Schematic diagram of 1D soil column infiltration test device (e) Schematic diagram of 2D model test device

Fig. 4 Test devices and their schematic diagrams

The data acquisition system receives and collects the test data. It consists of a water content sensor (accuracy 0.1%), matric suction sensor (accuracy 0.2%), pore pressure sensor (accuracy 0.2%), and intelligent data acquisition instrument. The devices and sensors used in the tests are illustrated in Fig. 5.

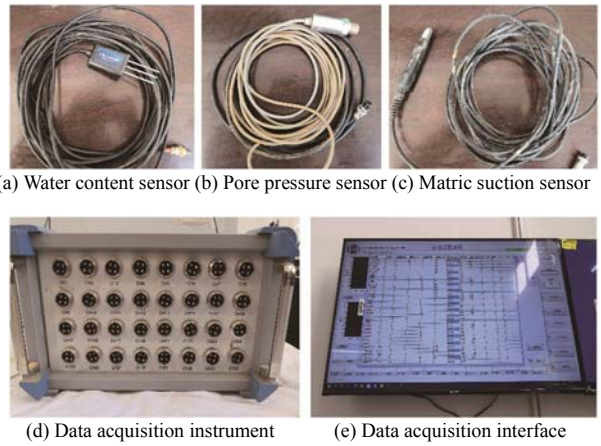

(a) Water content sensor (b) Pore pressure sensor (c) Matric suction sensor

(d) Data acquisition instrument (e) Data acquisition interface

Fig. 5 Data acquisition devices

3.2 Test soil samples

The test soil samples are obtained from a bank slope in the TGRA, and the soil samples are silty clay. This study mainly investigates the infiltration characteristics and deformation mechanism of landslide soil under different rainfall intensity to permeability coefficient (q/k) ratios. Considering the operability and

controllability of the test, for all the model soils in this study, the filling methods are kept the same to ensure that each group of test soils has the same physico-mechanical parameters. After filling the test soil samples (Fig. 6), their basic physico-mechanical parameters are obtained, as listed in Table 1.

3.3 Test schemes and steps

3.3.1 1D infiltration test

The 1D infiltration test simulates the vertical infiltration process of a 1D soil column with different rainfall intensities. Considering the rainfall capacity of the rainfall device, this study designs the corresponding rainfall intensity based on the ratio of the rainfall intensity to the saturated permeability coefficient of the soil sample. There are three groups (T1–T3) in this model test: the saturated permeability coefficient of the test soil is 78.1 mm/h, and when q/k is greater than 1, equal to 1, and less than 1, the rainfall is carried out under different rainfall intensities of 50, 80, and 100 mm/h until the soil sample is completely saturated. The experimental rainfall conditions are tabulated in Table 2.

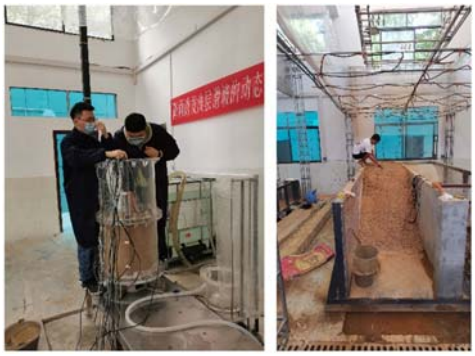

(a) 1D soil column test (b) 2D model test

Fig. 6 Soil filling in model tests

Table 1 Basic physico-mechanical parameters of test soil samples

Soil type	Unit weight /(kN • m^{-3})	Specific gravity	Dry density /(g • cm^{-3})	Initial water content /%	Cohesion /kPa	Internal friction angle /(°)	Saturated permeability coefficient /(mm • h^{-1})
Silty clay	19.71	2.687	1.43	13	8.54	31.87	78.1

Table 2 Test conditions for 1D infiltration test

Test condition	Rainfall intensity q /(mm • h^{-1})	Permeability coefficient k /(mm • h^{-1})	q/k
T1	50	78.1	0.66
T2	80	78.1	~1
T3	100	78.1	1.32

The test steps are described as follows:

(1) The inner wall of the cylinder is roughened with sandpaper to reduce the boundary effects.

(2) A layer of filter screen is placed at the bottom of the cylinder, and a layer of coarse gravel is added to prevent the bottom water outlet from being blocked. To ensure that each group of test soils has the same physico-mechanical parameters, the mass of the soil samples used in each group is kept the same, and the soil samples are filled in layers with the thickness of 5 cm for each layer. The soil samples are compacted by wooden circular plates, and the surface of each layer of soil is roughened to ensure that the connection of each soil layer is continuous. Then, each sensor is installed at a predetermined depth until the soil sample is buried to the required height (0.8 m), and a thin layer of small stones is laid on the top to prevent the disturbance by the rainfall.

(3) Each sensor is connected to the data acquisition instrument. The rainfall is initiated after setting the rainfall intensity in the rainfall system, and then the data and video are recorded simultaneously.

(4) The data changes of each sensor during rainfall are observed. After the soil sample is completely saturated and the data of each sensor are stable for a period of time, the rainfall is stopped and the test is terminated.

The total height of the soil column is 0.8 m, and the installed positions of the sensors for water content, matric suction, and pore air pressure are shown in Fig. 7. In addition, labels are attached to each depth outside the cylinder wall to facilitate the observation of the falling rate of the wetting front during the rainfall process.

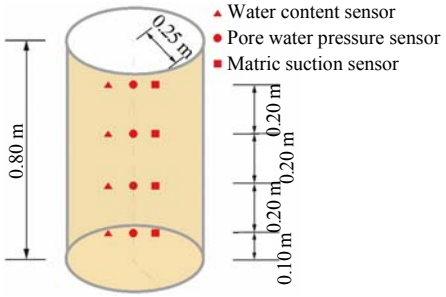

Fig. 7 Layout of monitoring sensors for soil column test

3.3.2 2D model test

Combining the results of the 1D model test and the 1D soil column infiltration test, the 2D model test examines two cases: q/k greater than 1 and q/k less than 1. The rainfall intensity in the 2D model test is consistent with the 1D infiltration test, and the rainfall continues until the landslide model is greatly deformed. The experimental rainfall conditions are listed in Table 3. The slope shape of the landslide model is convex, the bedrock is built with bricks and cement mortar, and the average slope angle is 20°. The sliding zone is made of talcum powder, bentonite, and heavy calcium carbonate mixed in proportion, and is evenly laid on the sliding bed with a thickness of approximately 3 mm. The landslide soil is placed in

layers, and the sensors are installed in the designed positions until a predetermined landslide shape is achieved.

The landslide model and arrangement of sensors are shown in Fig. 8. Five volumetric water content sensors and 5 pore air pressure sensors are installed 20 cm away from both sides of the model. The monitoring points on the left are numbered L1–L5, with L1, L3 and L4 buried at a depth of 0.5 m, L2 buried at a depth of 0.4 m, and L5 buried at a depth of 0.05 m. Five pore water pressure sensors and five matric suction sensors are installed in the middle of the model, numbered M1–M5. The buried depths of M1–M5 and R1–R5 correspond to L1–L5.

Table 3 Test conditions for 2D model test

Test condition	Rainfall intensity q /(mm • h^{-1})	Permeability coefficient k /(mm • h^{-1})	q/k
MODEL1	50	78.1	0.66
MODEL2	100	78.1	1.32

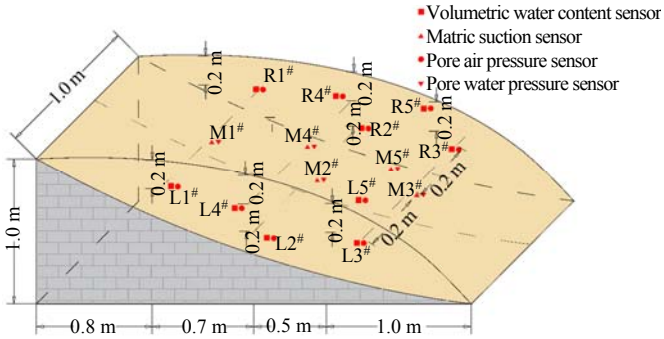

Fig. 8 Layout of monitoring sensors for 2D model test

4 Test results

4.1 1D soil column infiltration test

4.1.1 Test T1

For q/k<1, the wetting front processes during rainfall infiltration are shown in Fig.9, and the variations of the volumetric water content are shown in Fig.10(a). The time when the wetting front reaches each monitoring point is the same as the time when the water content at the monitoring point begins to vary. The time from the beginning of the water content change to the approximate saturation at each monitoring point is as follows: the water content at 0.1 m begins to increase at 1 200 s, reaches 36.5% at approximately 2 600 s and then stabilizes; the water content at 0.3 m begins to increase at 3 300 s, reaches 36.1% at approximately 5 000 s and then stabilizes; the water content at 0.5 m begins to increase at 6 000 s, reaches 39.5% at approximately 8300 s and then stabilizes; the water content at 0.7 m begins to increase at 9 600 s, reaches 39.9% at approximately 11 500 s and then stabilizes; after 12 000 s, rainwater infiltrates to 0.8 m at the bottom of the base.

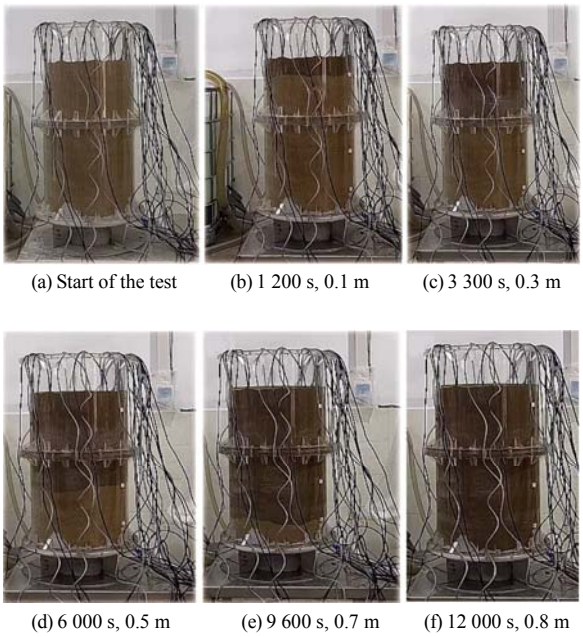

Fig. 9 Wet front processes during rainfall infiltration

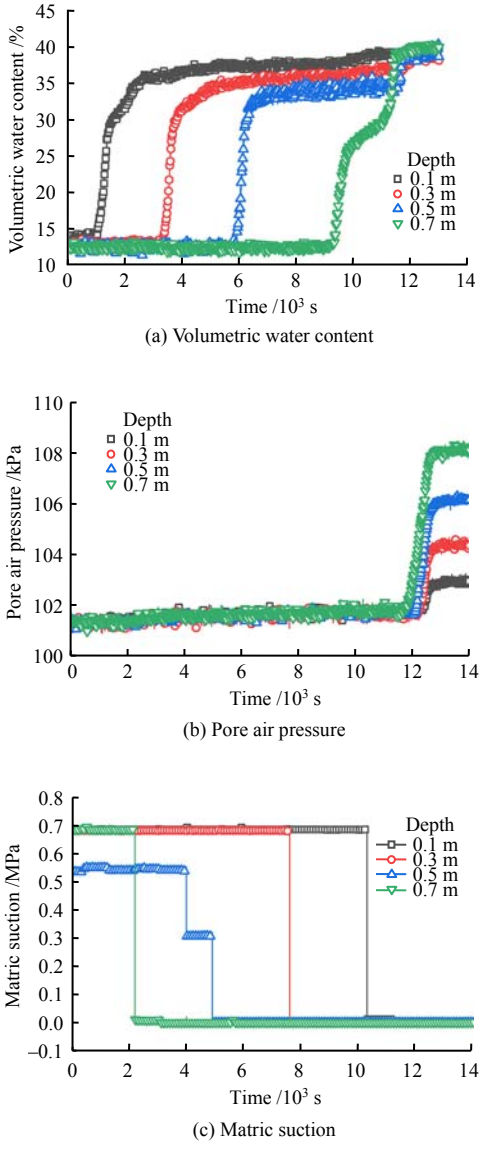

Fig. 10 T1 test results with rainfall intensity of 50 mm/h

Figure 10(b) shows the results of the change in pore air pressure. Because the bottom of the soil column test device is connected to the atmosphere during the rainfall infiltration, the pore air pressure maintains the atmospheric pressure at 101 kPa. After the rainfall lasts for 12 000 s, the pore air pressure at each measuring point gradually increases. The pore air pressure at 0.1 m increases by approximately 2 kPa, at 0.3 m by approximately 3 kPa, at 0.5 m by approximately 5 kPa, and at 0.7 m by approximately 7 kPa. The increase is consistent with the height of the water column. The reason for this analysis is that the water content at the bottom of the soil increases after 12 000 s of rainfall, and the surface and bottom soil masses are approximately closed. At this time, the water contents of the soils at different monitoring points are inconsistent, and the soil column does not reach a saturated state. An enclosed air space is formed inside. After the enclosed air is compressed by the water column, the pore air pressure increases, and the increase is identical to the water head at this location.

Figure 10(c) shows the results of the change in matric suction. The matric suction sensor has a high sensitivity to the water content, a large change rate, and a certain hysteresis compared to the water content. It cannot accurately reflect the influence of rainfall infiltration on the suction.

4.1.2 Test T2

When $q/k\approx1$, the wetting front process of rainfall infiltration is similar to that of Test T1. The variations of volumetric water content are shown in Fig. 11(a). The rainfall infiltration process is significantly faster than that of Test T1, and the test results are described as follows: the water content at 0.1 m begins to increase at 500 s, reaches 36.3% at approximately 2 000 s and stabilizes; at 0.3 m, it begins to increase at 2 300 s, reaches 37.3% at approximately 4 000 s and stabilizes; at 0.5 m, it begins to increase at 4 000 s, reaches 39.5% at approximately 6 200 s and stabilizes; at 0.7 m, it begins to increase at 5 600 s, reaches 39.9% at approximately 8 000 s and then stabilizes; after 9 000 s, the rainwater infiltrates to 0.8 m at the bottom of the base.

Figure 11(b) shows the changes in pore air pressure. The test phenomenon and the increase in pore air pressure are approximately the same as those in Test T1. Similarly, the increase in pore air pressure is identical to the water head. However, the pore air pressure increases at 4 200 s, which is significantly earlier than 12 000 s in Test T1. Figure 11(c) shows the changes in matric suction. One can see that the change in matric suction is the same as that in Test T1, but the time for this change is also significantly earlier than that in Test T1.

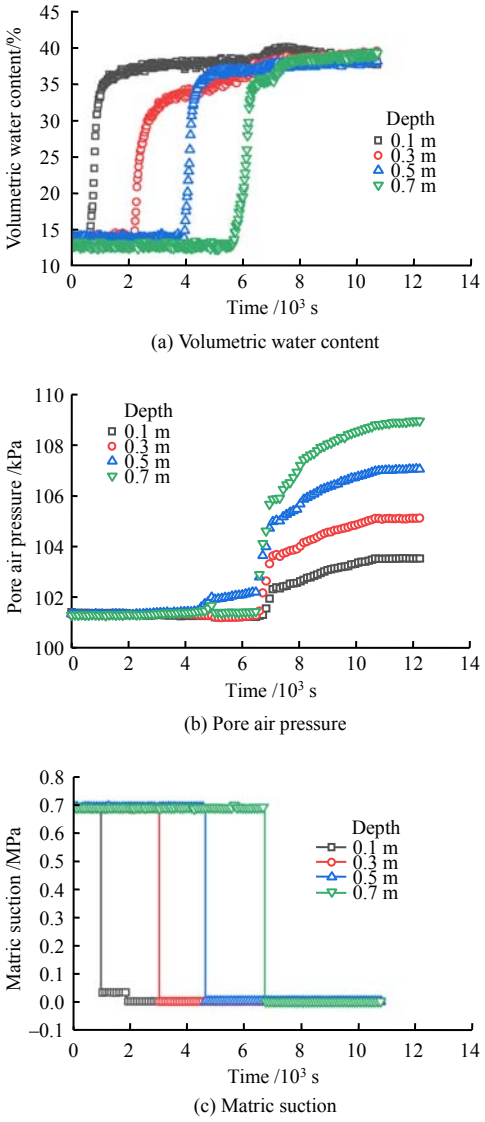

(a) Volumetric water content

(b) Pore air pressure

(c) Matric suction

Fig. 11 T2 test results with rainfall intensity of 80 mm/h

4.1.3 Test T3

The changes in volumetric water content at $q/k>1$ are shown in Fig. 12(a). The infiltration process is faster than that in Test T1, but significantly lags behind that in Test T2. In Test T3, the water content at 0.1 m increases at 1000 s, reaches 36.3% at approximately 2 200 s and then stabilizes; the water content at 0.3 m increases at 3500 s, reaches 36.9% at approximately 5 000 s and stabilizes; the water content at 0.5 m increases at 5000 s, reaches 36.8% at approximately 7 000 s and then stabilizes; the water content at 0.7 m increases at 6800 s, reaches 35.9% at approximately 8 000 s and stabilizes; after 10 000 s, the rainwater infiltrates to 0.8 m at the bottom of the base. Comparing the average volumetric water content of the four measuring points in each working condition, Test T2 is the largest, followed by Test T1, and Test T3, with the largest rainfall amount, is the smallest.

Figure 12(b) shows the changes in pore air pressure. After the rainfall lasting for 4000 s, the pore air pressure at each measuring point gradually increases. The pore air pressure at 0.1 m increases by approximately 2.5 kPa, at 0.3 m by approximately 4.5 kPa, at 0.5 m by approximately 6.5 kPa, and at 0.7 m by approximately 8.5 kPa, which exceed the results of Tests T1 and T2. Rainfall exceeding the permeability coefficient quickly formed stagnant water at the top. This results in an increase in the pressure of the enclosed air, and the magnitude of the increase is larger than the first two tests. It is observed that the time of increase of the pore air pressure is earlier than that in Test T1, but later than that in Test T2. Figure 12(c) shows the changes in matric suction. One can see that the change in matric suction is the same as that in Test T1, but the time when the matric suction decreases is earlier than that in Test T1 and later than that in Test T2.

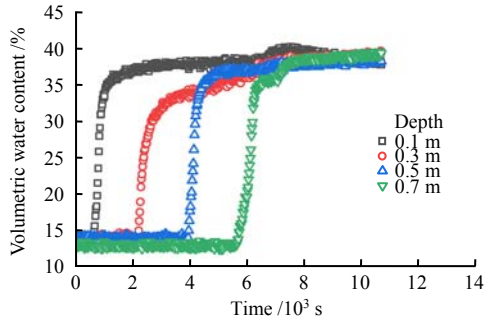

(a) Volumetric water content

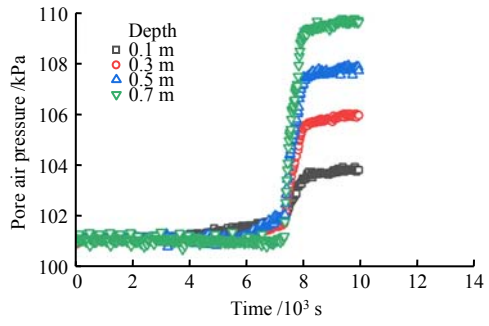

(b) Pore air pressure

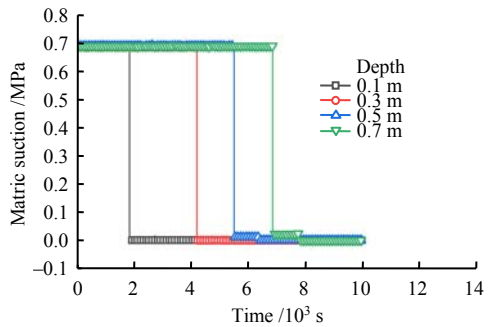

(c) Matric suction

Fig. 12 T3 test results with rainfall intensity of 100 mm/h

4.2 2D model tests

4.2.1 Model-1 with rainfall of 50 mm/h

The monitoring data of Model-1 test are shown in Fig. 13, and the images of several moments of sudden deformation in the landslide model are shown in Fig. 14. The change curves of water content in Fig. 13(a) show that the water contents at monitoring points L5 and R5, located in the middle and front surface of the landslide, first increase after approximately 1 000 s of rainfall; followed by the monitoring points L1 and R1, located at a depth of 0.2 m in the rear of the landslide (approximately 2 000 s), monitoring points L4 and R4 at a depth of 0.2 m in the middle (approximately 2 200 s), and finally the monitoring points L2 and R2 at a depth of 0.4 m in the middle (4 300 s). As shown in Fig.14(b), the tensile cracks begin to appear on the lower right side of the model at 4 800 s. Cracks further expand at 5 500 s (Fig. 14(c)) and are further damaged at 6 200 s (Fig. 14(d)). Correspondingly, before the three typical deformation cases, a sharp increase in water content occurs, as shown in Fig.13(a), corresponding to the two sudden changes of monitoring points L3 and R2, respectively. Evidently, the sharp increase in the internal water content is closely related to the shallow deformation of the landslide.

Figure 13(b) shows the monitoring results of the pore air pressure. The pore air pressures at the monitoring points L1 and R1, L5 and R5, and L4 and R4 located on the surface of the landslide do not appear to change significantly. However, the pore air pressures at the monitoring points L2, R2, L3, and R3, located in the deep part, begin to increase after approximately 3 000 s of rainfall, which also indicates that the rainfall infiltration forms a seal against the air, and the pore air pressure begins to gradually decrease after approximately 6 000 s, mainly because the deformation of the landslide affects the air tightness.

Figure 13(c) shows the monitoring results of pore water pressure. After the initial deformation of the landslide, the pore water pressures at the monitoring points M1, M2, and M4, located in the middle and rear of the landslide, increase significantly. The dominant seepage channel is generated by internal deformation, leading to an increase in rainfall infiltration and is also the main factor in the subsequent deformation of the landslide.

Figure 13(d) shows the monitoring results of the matric suction. Before the first deformation of the landslide, except for monitoring point M2 at a depth of 0.4 m in the middle, the other four monitoring points exhibit abrupt changes. Compared with other monitoring types, the early-warning of shallow deformation of the landslide by matric suction is more advanced.

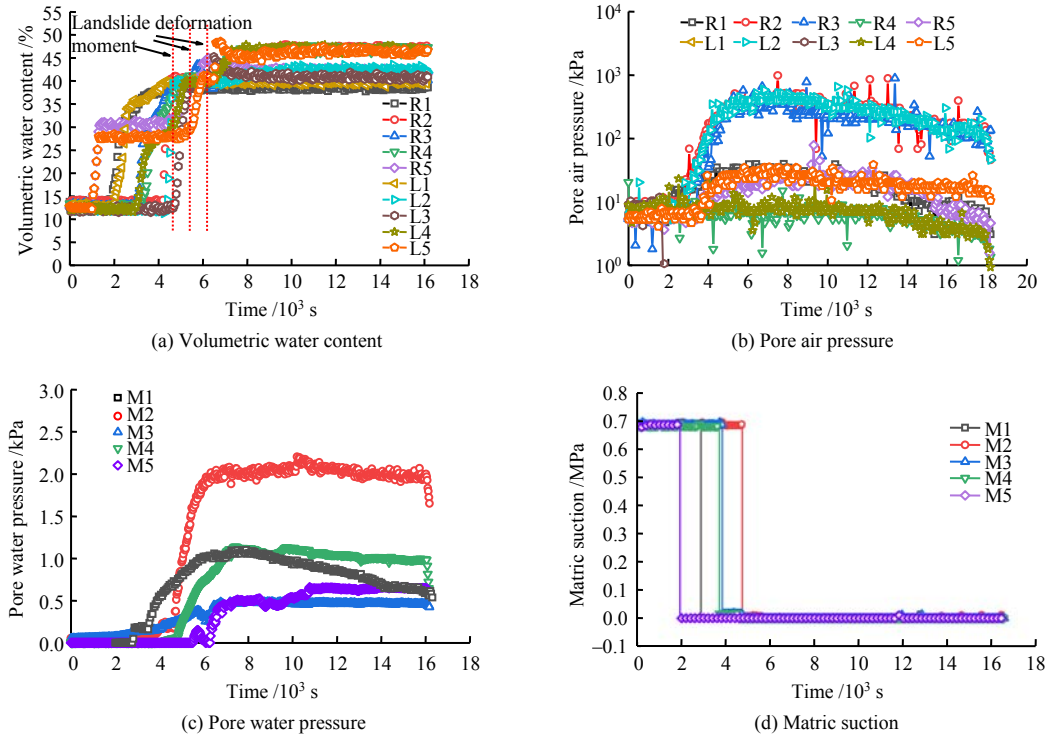

(a) Volumetric water content (b) Pore air pressure

(c) Pore water pressure (d) Matric suction

Fig. 13 Model-1 test results with rainfall intensity of 50 mm/h

(a) 0 s (b) Approximately 4 800 s (c) Approximately 5 500 s (d) Approximately 6 200 s

Fig. 14 Model deformation processes with rainfall intensity of 50 mm/h

4.2.2 Model-2 with rainfall of 100 mm/h

The monitoring data of Model-2 test are shown in Fig. 15, and the images of the deformation processes of the landslide model are shown in Fig. 16. Compared with the rainfall in the previous group of tests, the rainfall intensity in this group of tests is 100 mm/h, which exceeds the saturated permeability coefficient of the soil and is consistent with the results of the 1D soil column test. The infiltration rate of this group of tests is faster.

One can see from Fig.15(a) that the water content changes at each monitoring point are similar to those of the previous group of tests, but the time when the change occurs is earlier. Similarly, the sudden changes in water content correspond to several shallow deformation cases of the landslide. As shown in Fig.16(b), the tensile cracks begin to appear on the lower right side of the model at 2400 s, and the overall tensile deformation appears in the middle and front at 2600 s (Fig. 16(c)). At 2800 s, the cracks coalesce, and the middle and front of the model collapse (Fig. 16(d)). However, before the three typical deformation cases, the water content increases sharply, as shown in Fig. 15(a), corresponding to the monitoring points L3, R4, and R2, respectively. In the process of rainfall infiltration, with the deformation of the model, the cracks on the surface of the model also expand deeper, forming the dominant channel of rainfall infiltration. Therefore, the water content increases sharply, which leads to a sudden increase in pore water pressure (Fig. 15(c)), and the shear strength of soil decreases, resulting in the landslide deformation. The overall collapse of the model is associated with a sharp increase in the water content monitored by the monitoring point R2.

Figure 15(b) shows the monitoring results of the pore gas pressure. Similar to the results of the previous group of tests, the pore air pressures at the monitoring points located on the surface of the landslide do not change significantly. The pore gas pressures at the monitoring point R1, located in the middle and rear of

the model, begin to increase after approximately 2 000 s. Compared with the previous group of tests, the rainfall infiltration quickly seals the air, which does not dissipate significantly until the end of the test. The surface soil is saturated, and a sealing layer is formed.

Figure 15(c) shows the monitoring results of the pore water pressure. After approximately 2 000 s, the pore water pressure at the monitoring point M1 begins to increase, and the first deformation begins to appear at 2 400 s. At approximately 2 300 s, the pore water pressure at the monitoring point M2 increases sharply, and the value is close to 5 kPa. This is inconsistent with the pore pressure value at its depth (0.4 m), and its increased value is related to the transmission pressure of the pore air pressure. After 2 600 s, the landslide model fails. This failure is related to the increase in rainfall infiltration in the middle and rear of the model and the sudden increase in the pore water pressure at the monitoring point M2, resulting in an obvious hydrodynamic pressure and landslide failure.

Figure 15(d) shows the monitoring results of the matric suction. One can see that there is no obvious regularity in the changes in matric suction. However, at approximately 2 350 s, the matric suctions at the monitoring points M4 in the middle and M5 in the front of the landslide both change abruptly, corresponding to the first failure of the landslide at 2 400 s. Thus, the change in matric suction monitored can be used as an early- warning criterion for landslide deformation.

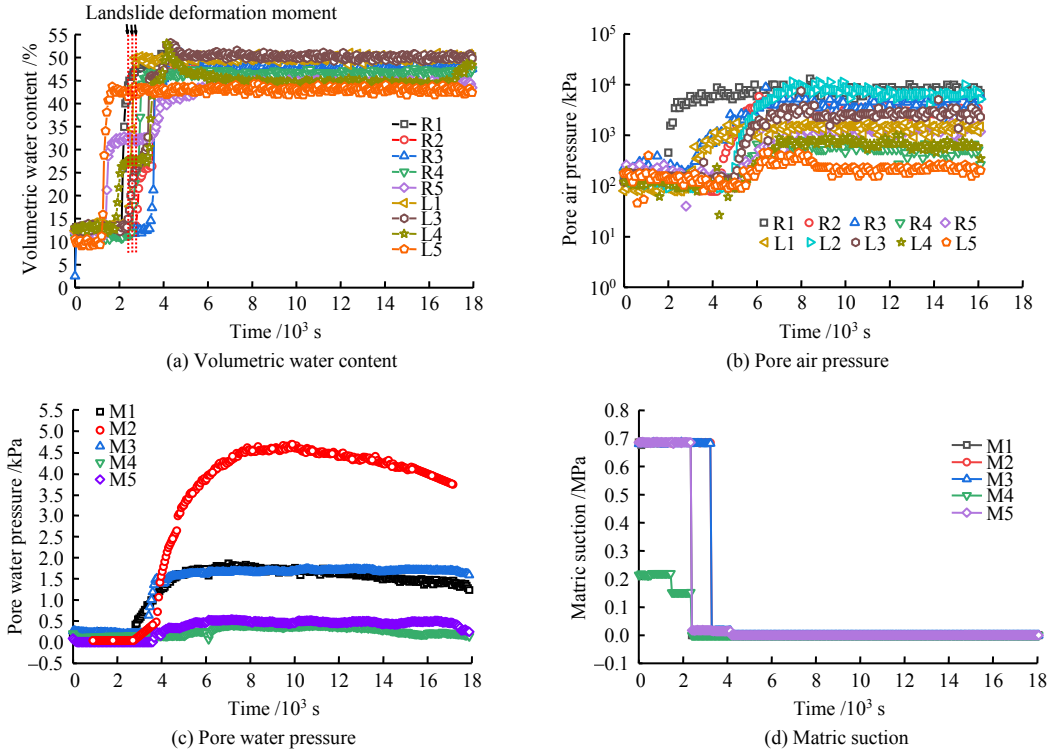

Fig. 15 Model-2 test results with rainfall intensity of 100 mm/h

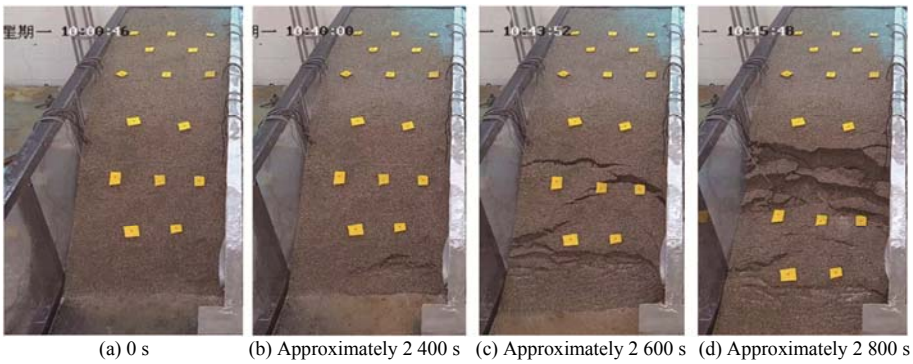

Fig. 16 Model deformation processes with rainfall intensity of 100 mm/h

5 Discussion

In the 1D test, three groups of rainfall infiltration tests with different q/k ratios are conducted. Different rainfall intensities show significant differences in infiltration capacity, and the infiltration capacity does not increase with increasing rainfall intensity. Figure 17 shows the time required to start infiltration to a certain

depth and to saturate the depth in the three 1D tests. As shown in Fig. 17, the infiltration rate in the Test T2 is the largest. Similarly, the time required for each monitoring point to reach saturation is the lowest. The Test T3, with the largest rainfall, has a similar infiltration rate to the Test T1 at the early stage, but is still significantly faster than that of the Test T1 in the later period. Through analyzing the time required for different depths of rainfall infiltration in three groups of tests in Fig. 17, there are also significant differences in the infiltration rates of soils at different depths. When $q \geqslant k$, the infiltration time of each position of the soil section is as follows: infiltration time from 0.5 m to 0.7 m < infiltration time from 0.3 m to 0.5 m < infiltration time from 0.1 m to 0.3 m; the infiltration rate is slow in the beginning, and the infiltration rate gradually increases as the depth increases. For $q < k$, the infiltration rates at each location are the opposite.

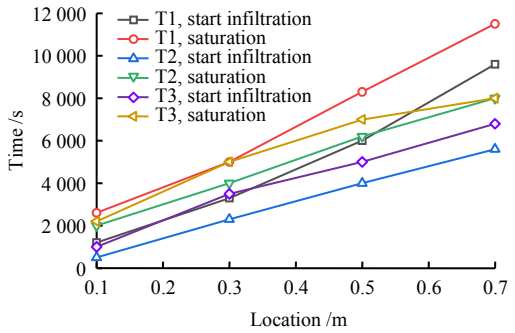

Fig. 17 Time-history diagram for 1D soil column infiltration

Rainfall exceeding the soil permeability coefficient reduces the infiltration rate of the rainwater. The main reason for this is that when rainfall is excessive, the stagnant water forms on the top of the soil column. As shown in Fig. 18, the rainfall causes the surface soil to be temporarily saturated, the air in the unsaturated area below the surface to be temporarily compressed, and the unsaturated area to be temporarily enclosed. The pore air is compressed, and the pore air pressure increases rapidly with the rainfall infiltration. This phenomenon is shown in the pore air pressure monitoring data of the 1D and 2D tests.

The sealed air can transfer the water pressure in the surface saturated zone to the underground aquifer. For example, in Model-1 and Model-2, the pore air pressure at the deep monitoring point begins to increase, and the subsequent increase in pore water pressure has an adverse effect on the stability of the landslide. In Model-2, the pore air pressure transfers the pore water pressure at the surface to a deeper position and significantly increases the pore water pressure at the bottom, resulting in the deformation of the landslide. Owing to the relatively closed spaces formed at the top and bottom, the pore air pressure dissipates slowly after the rainfall ceased. This innovative discovery highlights that in the slope stability research, the role of the pore air cannot be ignored, which changes the conventional understanding that the air barrier to the infiltration is beneficial to the slope stability. For the vast majority of landslides in the TGRA, short-term rainstorms cannot directly infiltrate the landslide body, but the resulting transient saturation zones cause the pore water pressure of the shallow soil to increase sharply, which is the main factor for the shallow deformation and failure of many landslides.

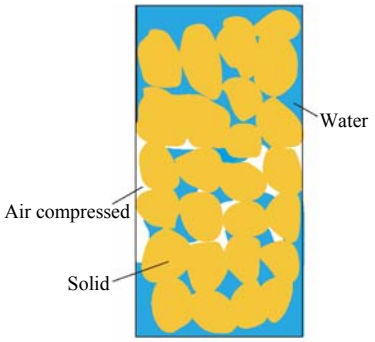

Fig. 18 Schematic diagram of air compression

6 Conclusions

(1) The speed of rainfall infiltration into the soil depends on the difference of the rainfall intensity and the soil permeability coefficient. When the rainfall intensity is less than or equal to the soil permeability coefficient, the infiltration capacity increases with increasing rainfall intensity. When the rainfall intensity is greater than the soil permeability coefficient, the infiltration capacity decreases.

(2) The infiltration of heavy rainfall causes transient saturation of the surface soil, and the air in the unsaturated zone below the surface is temporarily enclosed by the surface pore water pressure, which is the main factor affecting the infiltration capacity of heavy rainfall. Meanwhile, the enclosed air is compressed, resulting in a rapid increase in the pore air pressure with rainfall infiltration. Then the upper water pressure is transferred to sharply increase the pore water pressure of the soil under the enclosed air, which is the main factor for the shallow deformation and destruction of the ancient landslides in the TGRA.

This innovative discovery highlights that the role of the pore air cannot be ignored, which changes the conventional understanding that the air barrier to the infiltration is beneficial to the slope stability.

References

[1] TANG H M, WASOWSKI J, JUANG C H. Geohazards in the TGRA, China–lessons learned from decades of research[J]. Engineering Geology, 2019, 261: 105267.

[2] WANG L, CHEN Y S, WANG S M, et al. Response of

landslide deformation to rainfall based on multi-index monitoring: a case of the Tanjiawan landslide in the Three Gorges Reservoir[J]. Bulletin of Engineering Geology and the Environment, 2022, 81(6): 231.

[3] WANG S M, PAN Y C, WANG L, et al. Deformation characteristics, mechanisms, and influencing factors of hydrodynamic pressure landslides in the Three Gorges Reservoir: a case study and model test study[J]. Bulletin of Engineering Geology and the Environment, 2021, 80(4): 3513–3533.

[4] HOU T S, XU G L, ZHANG D Q, et al. Stability analysis of Gongjiacun landslide in the TGRA under the action of reservoir water level fluctuation and rainfall[J]. Natural Hazards, 2022, 114(4): 1647–1683.

[5] DING J X, YANG Z F, SHANG Y J, et al. A new method for spatial-temporal prediction of rainfall-induced landslide[J]. Science in China (Series D), 2006, 49: 421–430.

[6] WANG K, ZHANG S J. Rainfall-induced landslides assessment in the Fengjie County, Three-Gorge Reservoir Area, China[J]. Natural Hazards, 2021, 108(1): 451–478.

[7] DAMIANO E. Effects of layering on triggering mechanisms of rainfall-induced landslides in unsaturated pyroclastic granular soils[J]. Canadian Geotechnical Journal, 2019, 56(9): 1278–1290.

[8] MIAO F S, WU Y P, TRK K, et al. Centrifugal model test on a riverine landslide in the three gorges reservoir induced by rainfall and water level fluctuation[J]. Geoscience Frontiers, 2022, 13(3): 101378.

[9] BORDONI M, BITTELLI M, VALENTINO R, et al. Observations on soil-atmosphere interactions after long-term monitoring at two sample sites subjected to shallow landslides[J]. Bulletin of Engineering Geology and the Environment, 2021, 80(10): 7467–7491.

[10] ALONSO E, GENS A, LLORET A, et al. Effect of rain infiltration on the stability of slopes[C]//Proceedings of the First International Conference on Unsaturated Soils, UNSAT' 95. Paris: [s. n.], 1995, 241–249.

[11] ALVIOLI M, GUZZETTI F, ROSSI M. Scaling properties of rainfall induced landslides predicted by a physically based model[J]. Geomorphology, 2014, 213(15): 38–47.

[12] PERANIĆ J, MIHALIĆ A S, ARBANAS Z. Importance of the unsaturated zone in landslide reactivation on flysch slopes: observations from Valići Landslide, Croatia[J]. Landslides, 2021, 18(12): 3737–3751.

[13] PERANIĆ J, ARBANAS Ž. The influence of the rainfall data temporal resolution on the results of numerical modelling of landslide reactivation in flysch slope[J]. Landslides, 2022, 19(12): 2809–2822.

[14] DAS P, PATWA D, VISHNU G, et al. Influencing factors on the simulation of rainfall-induced landslide prediction based on case study[J]. Bulletin of Engineering Geology and the Environment, 2022, 81(5): 194.

[15] FANG K, MIAO M H, TANG H M, et al. Insights into the deformation and failure characteristic of a slope due to excavation through multi-field monitoring: a model test[J]. Acta Geotechnica, 2023, 18(2): 1001–1024.

[16] FANG K, MIAO M H, TANG H M, et al. Model test on deformation and failure behaviour of arching-type slope under excavation condition[J]. Engineering Geology, 2022b, 302: 106628.

[17] ZHOU Y Q, SHENG Q, CHEN J, et al. The failure mode of transmission tower foundation on the landslide under heavy rainfall: a case study on a 500-kV transmission tower foundation on the Yanzi landslide in Badong, China[J]. Bulletin of Engineering Geology and the Environment, 2022, 81(3): 125.

[18] HE C C, HU X L, DWAYNE D, et al. Response of a landslide to reservoir impoundment in model tests[J]. Engineering Geology, 2018, 247: 84–93.

[19] CHENG Y X, HUO A D, ZHAO Z X, et al. Analysis of loess fracture on slope stability based on centrifugal model tests[J]. Bulletin of Engineering Geology and the Environment, 2021, 80(5): 3647–3657.

[20] FANG K, TANG H M, LI C D, et al. Centrifuge modelling of landslides and landslide hazard mitigation: a review[J]. Geoscience Frontiers, 2023, 14: 101493.

[21] PECORARO G, CALVELLO M, PICIULLO L. Monitoring strategies for local landslide early warning systems[J]. Landslides, 2019, 16(2): 213–231.

[22] LI C D, LONG J J, LI Q, et al. Mechanism analysis and partition characteristics of a recent highway landslide in southwest china based on a 3D multi-point deformation monitoring system[J]. Landslides, 2021, 18(6): 2895–2906.

[23] CRAWFORD M M, BRYSON S L, WOOLERY E W, et al. Long-term landslide monitoring using soil-water relationships and electrical data to estimate suction stress[J]. Engineering Geology, 2019, 251: 146–157.

[24] BORDONI M, MEISINA C, VALENTINO R, et al. Hydrological factors affecting rainfall-induced shallow landslides: From the field monitoring to a simplified slope stability analysis[J]. Engineering Geology, 2015, 193: 19–37.

[25] TAKASHI O, SUMIO M, JAN O L, et al. The response of pore water pressure to snow accumulation on a low-permeability clay landslide[J]. Engineering Geology, 2018, 242: 130–141.

[26] WANG Li, LI Gao, CHEN Yong, et al. Field model test on failure mechanism of artificial cut-slope rainfall in Southern Jiangxi[J]. Rock and Soil Mechanics, 2021, 42(3): 846–854.

[27] CHEN Jian, YANG Zhi-fang, LI Xiao. Relationship between landslide probability and rainfall in TGRA[J]. Chinese Journal of Rock Mechanics and Engineering, 2005, 24(17): 3052–3056.

[28] American Standards for Testing and Materials. ASTM D6391－11. Standard test methods for field measurement of hydraulic conductivity using borehole infiltration[S]. West Conshohocken: American Standards for Testing and Materials, 2020.